UDC 669 . 14 . 018 . 295 . 2

Ultra High Tensile Strength Steel Cord

Hitoshi TASHIRO*(1)
Toshimi TARUI*(2)
Shoji SASAKI*(2)
Atsuhiko YOSHIE*(2)
Seiki NISHIDA*(2)
Shoichi OHASHI*(1)
Kenichi NAKAMURA*(2)
Hitoshi DEMACHI*(3)

Abstract

Commercialization of 0.20mm/4,000MPa ultra high tensile strength steel cord has been achieved by the improvement of ductility during wire drawing based on 0.9%C hypereutectoid steel wire rods. Although steel cord is used for belt and carcass parts of trucks and buses, the carcass parts of passenger car tires have been made of polyester. For the first time, 4,000MPa steel cord has been used for the carcass parts of passenger car tires. In the case of fine steel wire, strengthening by drawing is more effective than strengthening by patenting, and for 4,000MPa, the strengthening ratio by drawing reaches 65%. Clean hypereutectoid steel wire rods with little center segregation and undeformable inclusions are fundamental, but it is very important to have work hardening and wire uniform deformation at the time of fine drawing. This report describes the strengthening mechanism and improvement of ductility during wire drawing of hypereutectoid steel which has greatly contributed to the commercialization of 4,000MPa steel cord.

1. Introduction

Through the strong need for lighter weight in the automotive industry, the tensile strength of steel cord has been increasing steadily from its starting point of 0.20 mm/2,800 MPa class, and now 3,600 MPa class steel cord has been commercialized. Along with the striving for further improvements in high tensile strength, 4,000 MPa class has been developed[1-3] and commercialized by the 0.9%C hypereutectoid steel wire rod that is lower in center segregation and non-deformable inclusions and by the technologies for improving ductility through wire drawing. Because the strengthening ratio by drawing for 4,000 MPa class steel cord is 65%, which is even higher than the 3,600 MPa class, work hardening and uniform deformation of wire are extremely important when drawing fine steel wire. This report describes the strengthening mechanism of hypereutectoid steel and improvements in ductility through wire drawing that have contributed greatly to the commercialization of 4,000 MPa class steel cord.

2. Strengthening Mechanism of Hypereutectoid Steel[4]

In order to quantify the effects of carbon content on the strength of wire, we tried formulating the work hardening of hypereutectoid steel wire during drawing. For this objective, analysis of the true stress and true strain curves and detailed observation of microstructure were done, and as a result, a formula expressing the relationship between flow stress and strain was developed. Using the attained formula for estimating work hardening, the strengthening mechanism of hypereutectoid steel was investigated. This paper also introduces the suggestion that the strength of wire after drawing can be estimated by using this formula.

2.1 Formulation of work hardening by wire drawing

The 1.7 mm diameter wire, the chemical composition of which is indicated in **Table 1**, was patented at the isothermal transformation temperature of 570°C and was drawn up to 0.3 mm in diameter. The true stress and true strain curves of the wire obtained in this process

*(1) Kamaishi Works
*(2) Technical Development Bureau
*(3) Kimitsu Works

Table 1 Chemical compositions of steel used in the test

Steel types	Chemical compositions (mass %)					
	C	Si	Mn	P	S	Cr
S82A	0.83	0.20	0.52	0.005	0.013	0
92ACr	0.92	0.21	0.30	0.005	0.007	0.20

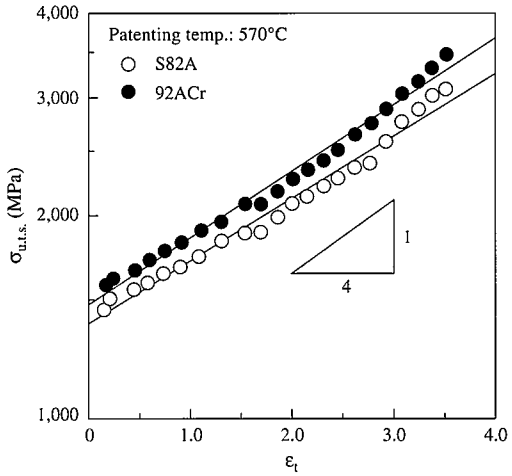

Fig. 1 Work hardening curve of wire isothermally transformed at 570°C

were found and the total strain ε_t (sum strain by the tensile test and by drawing) and the ultimate tensile strength $\sigma_{u.t.s.}$ were found. **Fig. 1** shows the relationship between ε_t and $\sigma_{u.t.s.}$. Applying the conventional relationship[5] where $\sigma_{u.t.s.}$ is proportional to exp (ε_t/4), the increase of work hardening in the high strain region and the effect of carbon content cannot be completely explained.

There, the strength σ of pearlite is assumed to be expressed with a weighted average[6] of the strengths of cementite and ferrite as equation (1).

$$\sigma = V_\theta\sigma_\theta + V_\alpha\sigma_\alpha \quad \cdots\cdots (1)$$

Here, V_θ is the volume fraction of cementite, σ_θ is the strength of cementite, V_α is the volume fraction of ferrite and σ_α is the strength of ferrite. We used the fracture strength that Webb et al.[7] found from the cementite extracted from pearlite to hypothesize the flow stress σ_θ of cementite at a fixed 8,000 MPa.

Next, ferrite deformation stress σ_α is expressed by equation (2)[8].

$$\sigma_\alpha = \sigma_{\alpha 0} + \alpha\mu b\sqrt{\rho} \quad \cdots\cdots (2)$$

Here, $\sigma_{\alpha 0}$ is the frictional stress of ferrite (59 MPa[9]), α is the constant, μ is the elastic modulus, b is the size of the Burgers vector and ρ is the dislocation density. Equation (3) is obtained by substituting equation (2) into equation (1).

$$\sigma = V_\theta\sigma_\theta + V_\alpha\sigma_{\alpha 0} + V_\alpha\alpha\mu b\sqrt{\rho} \quad \cdots\cdots (3)$$

Because the first and second terms on the right of equation (3) are constants, the work hardening of ferrite is obtained by subtracting the first and second term from the flow stress σ of the pearlite on the left side. In other words, transforming equation (3) so that the left side is $(\sigma - V_\theta\sigma_\theta - V_\alpha\sigma_{\alpha 0}) / V_\alpha$, it is easier to obtain the value of $\alpha\mu b\sqrt{\rho}$ by calculation.

ln ($\alpha\mu b\sqrt{\rho}$) obtained from the various data of Fig. 1 has been plotted for ε_t in **Fig. 2**. ln ($\alpha\mu b\sqrt{\rho}$) becomes larger in proportion to ε_t. This relationship is shown in equation (4).

$$\alpha\mu b\sqrt{\rho} = K \exp(B\varepsilon_t) \quad \cdots\cdots (4)$$

The dislocation density resulting in work hardening is hypothesized to be expressed[10] as equation (5) using the width S_α of ferrite taken up in the lamellar spacing.

$$\rho = 3/S_\alpha^2 \quad \cdots\cdots (5)$$

The change of the lamellar spacing is expressed by equation (6)[5].

$$S_\alpha = S_{\alpha 0} \exp(\varepsilon_t/2) \quad \cdots\cdots (6)$$

Here, $S_{\alpha 0}$ is the width of ferrite taking up in the initial lamellar spacing. A combination of equation (5) and equation (6) obtains the equation (7).

$$\alpha\mu b\sqrt{\rho} = (\sqrt{3}\alpha\mu b/S_{\alpha 0}) \exp(\varepsilon_t/2) \quad \cdots\cdots (7)$$

Comparing equation (4) with equation (7), it is derived that K is in proportion to the inversion of the lamellar spacing and the value of B is 0.5.

When the isothermal transformation temperature was changed from 530°C to 590°C to change the volume ratio of pearlite, the values of B in equation (4) were found. **Fig. 3** shows the results. V_p in Fig. 3 expresses the volume fraction of pearlite, and the remainder of 1–V_p is the volume fraction of upper bainite. When microstructure is only pearlite, in other words $V_p = 1$, it is understood, then, that the value of B is 0.5 as stated earlier. From the above considerations, the work hardening of pearlite during drawing is expressed by the following equation.

$$\sigma = V_\theta\sigma_\theta + V_\alpha\{\sigma_{\alpha 0} + (\sqrt{3}\alpha\mu b/S_{\alpha 0}) \exp(\varepsilon_t/2)\} \quad \cdots\cdots (8)$$

Because the volume fraction of ferrite and the volume fraction of

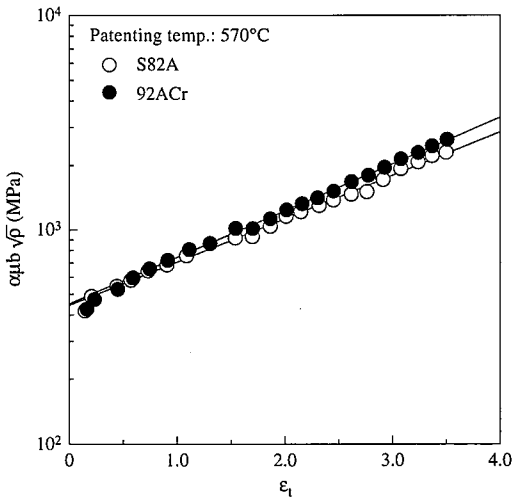

Fig. 2 Relationship between strain and work hardening of ferrite

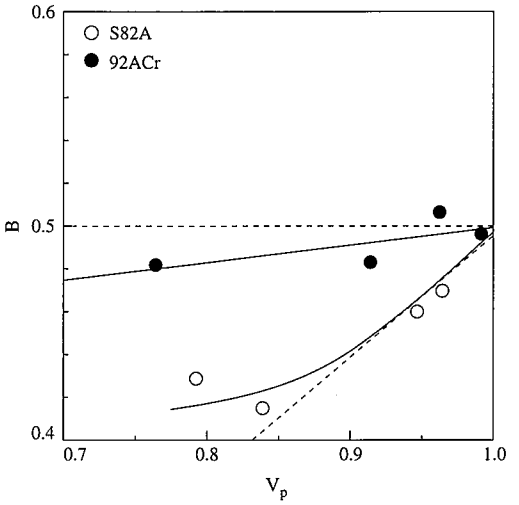

Fig. 3 Relationship between pearlite volume fraction and the value of B

cementite can be obtained from the equilibrium state, substituting known values into equation (8) allows us to arrive at equation (9).

$$\sigma = 59 + 1{,}253[C\%] + (2.228 \times 10^{-5}/S_{\alpha 0}) \exp(B\varepsilon_t)\} \cdots\cdots (9)$$

[C%] : Carbon content (mass %)

$S_{\alpha 0}$: Width of ferrite occupied in initial lamellar spacing (nm)

ε_t : Total strain (true strain)

B : Constant depending on microstructures

However, with only pearlite, it is B = 0.5; and if pearlite contains upper bainite, it is B < 0.5.

2.2 Comparison of estimating formulas and experimental results

Wire that was patented (at the isothermal transformation temperature of 570°C) in which the pearlite was more than 95% of the structure after the isothermal transformation was drawn. The flow stress of wire adjusted to the work amount at each stage is shown in **Fig.4** with SWRS 82A (described as S82A below) by ○ and 92ACr by ●. Furthermore, each work hardening curve of S82A and 92ACr is shown as a solid line in Fig. 4, which is obtained by substituting the carbon content, the measured interlamellar spacing and 0.5 as the value of B in equation (9). When the pearlite fraction is more than 95%, it shows that the actual flow stress of the wire agree with the flow stress obtained using equation (9) in both cases of S82A and 92ACr.

Next, wire was patented (at the isothermal transformation temperature of 530°C) in which pearlite was less than 95% of the structure after isothermal transformation was drawn. The flow stress of wire that was adjusted to the work amount at each stage is shown in **Fig. 5** using ○ for S82A and using ● for 92ACr. Also, each work hardening curve of S82A and 92ACr is shown by a solid line in Fig. 5. This is obtained by substituting the carbon content, the measured interlamellar spacing and 0.5 as the value of B in equation (9). When the pearlite volume fraction is less than 95%, flow stress attained from the calculation is larger than the actual flow stress of the wire. Also, compared to 92ACr, S82A shows a greater difference between the actual deformation stress of the wire and the calculated value from equation (9).

Using the value of B estimated from the relationship between the pearlite volume fraction and the value of B shown in Fig. 3, the work hardening curve was obtained from equation (9), which is shown as the broken line in Fig. 5. In this case, it is clear that the experimental values agree with the calculated values and are good matches.

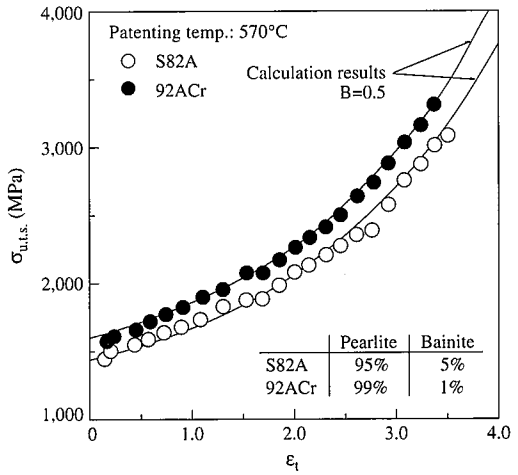

Fig. 4 Comparison between experimental values of pearlite steel wire and calculated valuesg

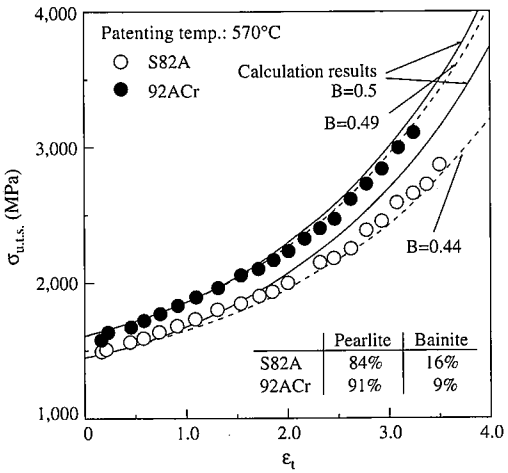

Fig. 5 Comparison between experimental values of pearlite steel wire containing higher fraction of upper bainite and calculation results

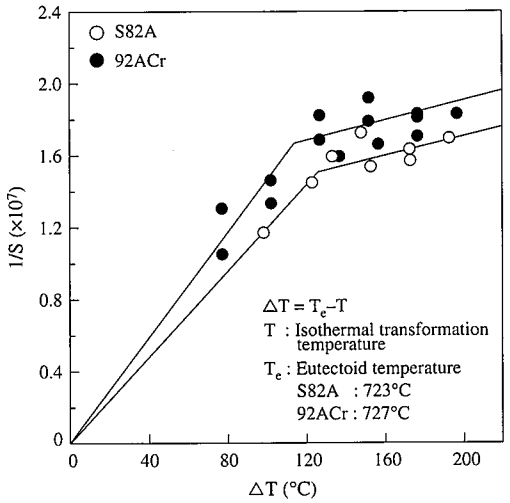

Fig. 6 Relationship between super cooling ΔT and lamellar spacing

2.3 Strengthening mechanism of hypereutectoid steel

Comparing the work hardening of S82A with hypereutectoid steel 92ACr obtained by derived equation, we know that three strengthening mechanisms are at work in 92ACr. Namely:

(1) Because the volume ratio of cementite is higher in 92ACr than in S82A, the strength is higher in proportion to carbon content as shown in equation (9). This increased strength does not affect work hardening.

(2) Because interlamellar spacing after isothermal transformation is smaller in 92ACr than in S82A, as is shown in **Fig. 6**, work hardening is greater.

(3) Because the decrease of the value of B resulting from the appearance of upper bainite is smaller in 92ACr than in S82A, as is shown in Fig. 3, work hardening of commercial patented wire is greater in 92ACr.

2.4 Application to estimating strength

Fig. 7 shows the result of work hardening of S82A and 92ACr calculated by equation (9). From this curve, it was estimated that patented wire diameter producing 0.2 mm/3,600 MPa wire would be 1.36 mm for S82A and 1.17 mm for 92ACr. It was estimated that patented wire diameter producing 0.2 mm/4,000 MPa wire would be 1.46 mm for S82A and 1.38 mm for 92ACr.

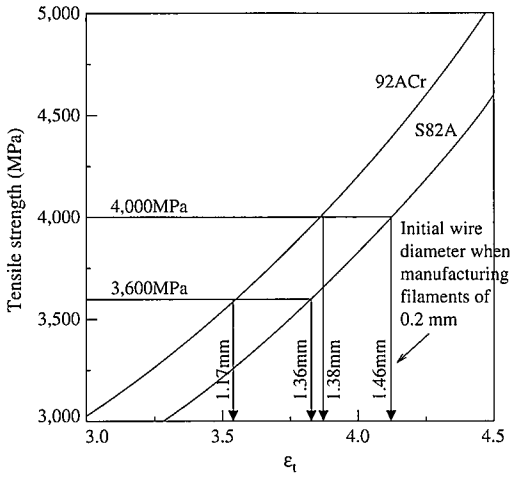

Fig. 7 Relationship between the strength of wire after drawing and strain

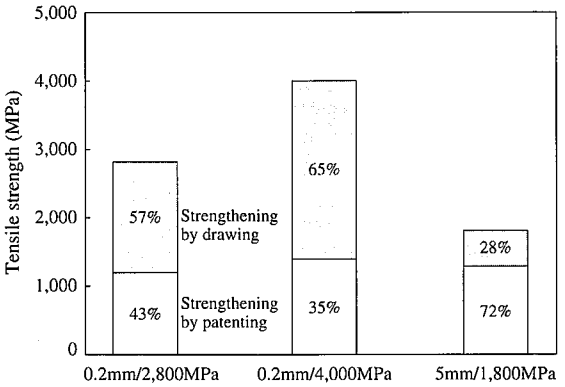

Fig. 8 Comparison of strengthening by patenting and drawing in the tensile strength of wire

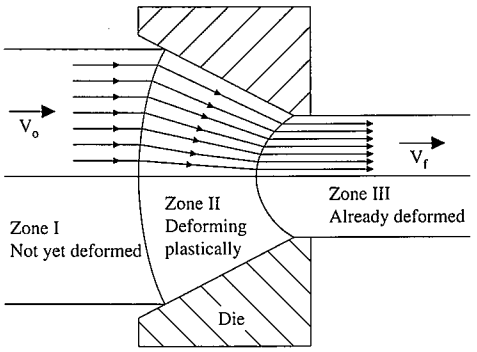

Fig. 9 Scheme of wire plastic deformation during drawing wire using die

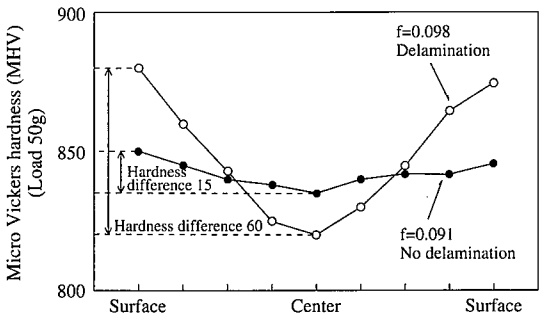

Fig. 10 Influence of the friction coefficient affecting the cross section hardness distribution of 0.30 mm fine steel wire

3. Technology for Improving Ductility through Wire Drawing

3.1 Philosophy of improvements of ductility through drawing fine wire

Steel cord is 2 to 39 pieces of twisted, 0.15 to 0.38 mm brass plated wire drawn with wet lubrication using WC dies or diamond dies. **Fig. 8** shows the patenting and wire drawing strength ratios of fine and thick diameter wire. With fine wire, the strength ratio of wire drawing is large so it is important to the uniform deformation of wire and the work hardening ratio.

With the die drawing shown in **Fig. 9**, the position at which the plastic deformation starts differs for the surface layer and the center of wire, resulting in non-uniform deformation[11]. Because the surface layer is more deformed, it is more work hardened. When non-uniform deformation occurs, there is a decrease in ductility such as delamination, torsion values and elongation. Strain aging when drawing fine wire degrades ductility, but because this is done with wet lubrication, it is hypothesized that there is little effect. In order to attain high tensile strength, the pearlite lamellar spacing of patenting material must be finer and it is necessary to increase the strain of wire drawing along with increasing tensile strength and work hardening ratio[3].

First is the philosophy of improvements of ductility through drawing fine wire by analyzing the drawing force during die drawing. There are several formulas for drawing force[12]. The one used most prevalently is Siebel's formula (10).

$$Z = s \cdot \varepsilon \cdot R\,(1 + 2f / \theta + \theta / 3\varepsilon) \quad \cdots\cdots (10)$$

Drawing force = effective deformation work + external frictional work + shearing work

Z : Drawing force
R : Average deformation resistance
s : Wire cross-sectional area after drawing
f : Friction coefficient between die and wire
ε : Wire drawing strain [ln $(d_0/d_n)^2$]
θ : Die approach angle (full angle)
d_0 : Wire diameter before drawing
d_n : Wire diameter after drawing

The ratio of each work will vary according to the angle of the die approach, and an angle that gives the smallest drawing force exists. Up to now, drawing conditions where the drawing force is smallest were the optimum[13]. However, drawing conditions where the drawing force is the smallest does not necessarily get maximum uniform deformation. Reduction of die approach angle and friction coefficient promote a more uniform deformation.

Fig. 10 shows an example of the effect that the friction coefficient exercises on the uniform deformation of 0.30 mm fine steel wire. A hardness distribution of the cross-section of wire was used as an index for uniform deformation. There is uniform deformation as the difference in hardness between the surface and the center decreases. The distribution of hardness of the cross-section of wire is V-shaped, and hardness increases as much as the surface. Reduction of the friction coefficient promotes uniform deformation and the difference in hardness decreases. The promotion of uniform deformation prevents the occurrence of delamination. It is necessary to contrive like the carrier, the lubricant, die material, shape and reduction ratio

for each pass when drawing fine wire in order to promote uniform deformation.

3.2 The effect of brass plating carrier

A effect of brass plating carrier has a great effect on uniform deformation during drawing fine wire. In the case of steel cord, fine wire drawing is performed after brass plating, and there are carrier effects during fine wire drawing as well as adhesion with the tire rubber in the brass plating[14]. When there is no plating, zinc phosphate is commonly used as the carrier. As shown in **Fig. 11**, brass plating has more superior lubricating performance with higher ultimate strength at which delamination does not occur. Also, we saw the thickness effects of the brass plating. It is necessary to increase the plating thickness to increase the strain of wire drawing.

The friction coefficients between the die and wire during fine wire drawing with wet type lubrication using diamond dies are 0.093 for brass plating and 0.11 for zinc phosphate. So it is clear that brass plating is lower. As shown in **photo 1**, the brass plated surface has much more unevenness than zinc phosphate, and regions of boundary lubrication are finely dispersed. Because it is known that oil components and the extreme-pressure additive of wet lubricant adhere to the metal, creating an adhering film, thereby reducing the friction coefficient[15], brass plating is also advantageous in that point as well. **Table 2** shows the features of brass plating and zinc phosphate.

Fig. 12 shows a depth profile analysis of brass plated fine steel wire using the Auger electron spectroscopy, and **Fig. 13** shows the change of surface Fe concentration when drawing fine brass plated wire. As wire drawing strain increases, the concentration of Fe increases. Along with the wire drawing, the diameter of the wire thins, so there is an increase in specific surface area. For that reason, it is essential that internal atoms come to the surface. Because the brass plating is a thin 2 to 3 μm, it is considered that the internal Fe comes to the surface. A concentration gradient can be seen in the brass plating, in Fig. 12, and there is an increase in Fe concentration as it moves internally. It is considered that as the surface layer Fe concentration increases, brass plating becomes harder and there is a

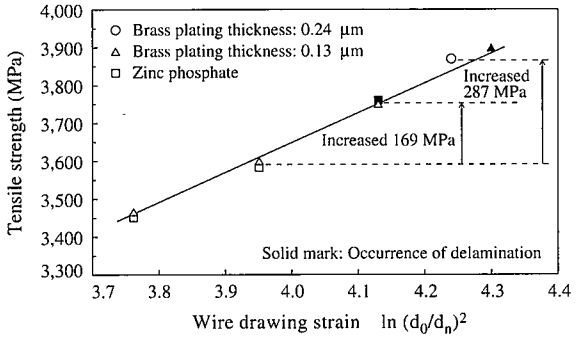

Fig. 11 Influence of the carrier affecting the maximum ultimate strength of 0.30 mm fine steel wire

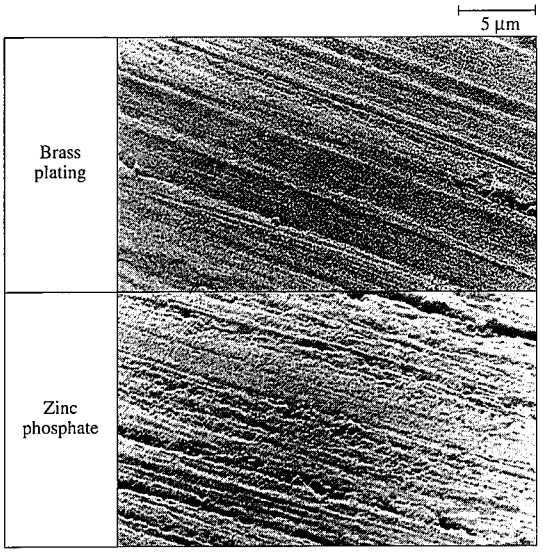

Photo 1 Influence of the carrier affecting the surface of 0.30 mm fine steel wire

Table 2 Comparison of brass plating as a carrier and zinc phosphate

	Brass plating	Zinc phosphate
Chemical compositions	Cu70%-Zn30%	$Zn_3(PO_4)_2$ Zn: 51%
Carrier surface status	Faithfully reflecting surface state of steel wire	Crystals precipitate without being affected by surface state of steel wire
MHV	174	114
Others	1.Reaction of oils and extreme pressure agent creates attraction film 2.Great plastic deformability	Precipitation by chemical reaction accompanying hydrolysis forms firm carrier

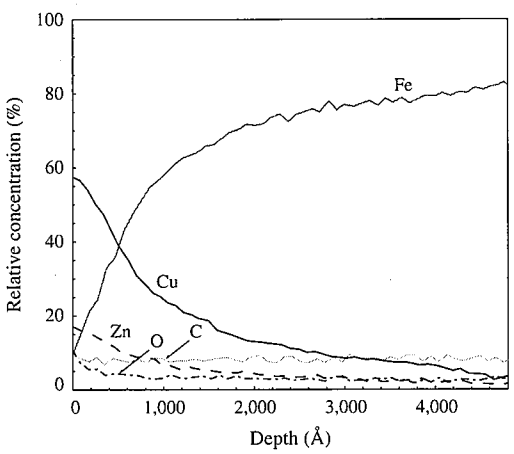

Fig. 12 Depth profile analysis in 0.30 mm brass plated fine steel wire using Auger electron spectroscopy

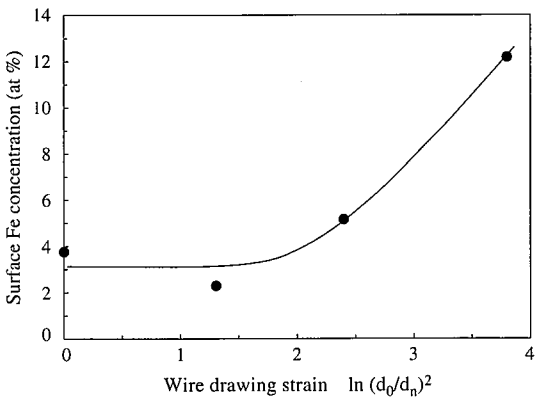

Fig. 13 Influence of wire drawing strain affecting surface Fe concentration in 0.30 mm brass plated fine steel wire

degradation of the carrier effect. When strengthening, there is an increase in wire drawing strain, so increasing brass plating and restricting the increase of surface Fe concentration is effective in improving ductility.

3.3 Technology for improving ductility through drawing fine wire

As mentioned above, one effective method of promoting uniform deformation when drawing fine wire is the low die angle approach. By lowering the angle from 14 degrees to 10 degrees, the micro Vickers hardness difference between the surface and the center in cross section will become smaller to homogenize the distribution. Furthermore, in promoting uniform deformation, wire drawing with low reduction of less than 10% during the final stage is effective. The combination of a low approach die angle and the wire drawing with low reduction during the final stage are effective. (See **Fig. 14**)

Other than the low approach die angle and the wire drawing with low reduction during the final stage there is also the technology for improving ductility after wire drawing. By promoting the lowering of yield stress and softening of the surface, it is possible to attain the same effect as promoting uniform deformation[16]. One is roll straightening technology. This is effective not only for thick diameter wires, but also for fine wire and if bending strain and back tension on the fine wire is controlled, there can be an improvement in ductility without lowering tensile strength. (See **Fig. 15**)

3.4 High strengthening by 0.9% C hypereutectoid steel wire and technology for improving ductility through wire drawing

As can be seen in **Table 3**, 0.20 mm/4,000 MPa class wire with

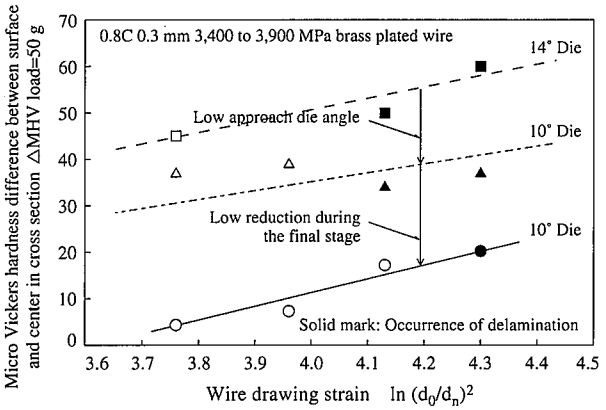

Fig. 14 Influence of die approach angle and low reduction during the final stage affecting wire cross section micro Vickers hardness distribution in fine steel wireg

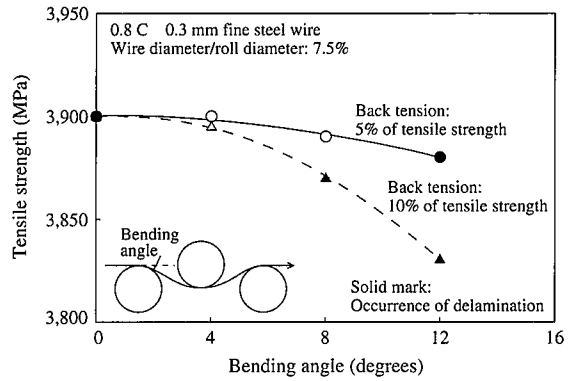

Fig. 15 Influence of roll straightening conditions affecting tensile strength of fine steel wire and delamination

Table 3 Characteristics of 0.20 mm/4,000 MPa class brass plated fine steel wire

Steel type	Chemical compositions (mass %)					
	C	Si	Mn	P	S	Cr
SWRS 92A	0.92	0.22	0.48	0.014	0.008	—
92ACr	0.91	0.20	0.31	0.006	0.007	0.20

Quality of 5.5 mm wire rod		Mechanical properties of 0.20 mm brass plated fine steel wire			
Segregation index	Non-deformable inclusion index	Tensile strength (MPa)	Torsion value (times, l=100 d*)	Delamination	Micro Vickers hardness difference between cross section surface and center
0	1	4,012	27	None	15
0	1	4,008	28	None	13

*d: Wire diameater

no delamination and high ductility can be attained by a combination of the technology for improving ductility through such methods as brass plating, low approach die angle and wire drawing with low reduction during the final stage with the 0.9%C hypereutectoid steel wire that is low in center segregation and nonmetallic inclusions. Through this method, 4,000 MPa class steel cord has been used for the first time in the carcass of tires for passenger cars.

4. Conclusion

Commercialization of 0.20mm/4,000MPa class steel cord has been achieved from 0.9%C hypereutectoid steel wire that is low in center segregation and non-deformable inclusions and using technologies for improving ductility through wire drawing. Thus, steel is being used for the first time in the carcasses of passenger car tires. Hypereutectoid steel strengthening mechanisms and technology for improving ductility through wire drawing have contributed to the commercialization of the 4,000 MPa class. Because strengthening through wire drawing is dominant in fine wires, high work hardening ratios and uniform deformation of wire are extremely important to maintain high ductility. It is considered that the need for even lighter weights will increase, so there still remain the challenges of promoting development in both steel materials and wire drawing technology to the limits of their strength.

References

1) Ochiai, I., Nishida, S., Tashiro, H.: Wire J. Int. 26(12), 50(1993)
2) Takahashi, T., Ochiai, I., Tashiro, H., Ohashi, S., Nishida, S., Tarui, T.: Shinnittetsu Giho. (354), 39(1994)
3) Tarui, T., Takahashi, T., Tashiro, H., Nishida, S.: Metallurgy, Processing and Applications of Metal Wires. TMS, 1996, p.87
4) Nishida, S., Yoshie, A., Imagumbai, M.: Trans. ISIJ. 38(2), 177(1998)
5) Langford, G.: Metall. Trans. 8A, 861(1977)
6) Sudo, H.: Bull. Japan Inst. Metals. 9, 3(1970)
7) Webb, W. W., Forgeng, W. D.: Acta Metall. 6, 462(1958)
8) Bailey, J. E., Hirsch, P. B.: Philos. Mag. 5, 485(1960)
9) Lacy, C. E., Gensamer, M.: Trans. Am. Soc. Met. 32, 88(1944)
10) Takagi, S.: Strengthening Mechanism and Strengthening Theory of Steel. 141st Nishiyama Memorial Technical Lecture, ISIJ, 1992, p.1
11) Avitzur, B.: Wire J. Int. 7(11), 77(1974)
12) Gokyu, I. Translation, Geleji, A.: Calculations of Metal Plastic Forming (II), Korona Sha, Japan, 1994, p.25
13) JSTP: Drawing. Korona Sha, Japan, 1990, p.17
14) Sasaki, S., Tashiro, H.: Wire J. Int. 31(7), 104(1998)
15) Nippon Yushi: Surfactant Handbook. Kogakutosho, Japan, 1987, p.326
16) Takahashi, T., Ohashi, S., Tarui, T., Asano, G.: Shinnittetsu Giho. (347), 22(1992)